ARCHIVES OF ELECTRICAL ENGINEERING VOL. 75(1), pp. 79 –102 (2026)

DOI 10.24425/aee.2026.156803

A modified geometric mean optimizer for integrating distributed photovoltaic power generation into radial distribution networks

Ghassan Abdullah Salman [1,2]✉, **Layth Tawfeeq Al-Bahrani** [1]

[1] *Department of Electrical Engineering, College of Engineering, Mustansiriyah University Iraq*

[2] *Department of Electrical Power and Machines, College of Engineering, University of Diyala Iraq*

e-mail: {✉ ghassanabdullah/laith1973a}@uomustansiriyah.edu.iq

(Received: 13.08.2025, revised: 23.01.2026)

Abstract: This paper proposes a modified geometric mean optimizer (MGMO) based on nonlinear functions of the control parameter, the first being a logarithmic function (MGMOI) and the second being an exponential function (MGMOII), while the original geometric mean optimizer (OGMO) has a linear control parameter. To demonstrate the effectiveness and efficiency of an MGMOI and MGMOII, they were implemented to benchmark functions, the results observed a best balance in exploration and exploitation and faster convergence to the best solution compared to the OGMO. On the other hand, the OGMO, MGMOI and MGMOII algorithms have been implemented on the standard IEEE 33 bus and the practical IRAQI 71 bus to obtain the optimal position and capacity of photovoltaic distributed generator (PV-DG), while the beta probability distribution function (BPDF) is implemented to model the uncertainty of solar irradiation. Moreover, the performances of radial distribution networks (RDNs) are improved after incorporating a PV-DG into the RDN; the power losses are minimized (65.159%, 65.500%, and 65.505% for the OGMO, MGMOI, and MGMOII, respectively, in the IEEE 33 bus, 66.739%, 66.858%, and 67.490% for the OGMO, MGMOI, and MGMOII, respectively, in the IRAQI 71 bus), while the voltage profile and stability are maximized (15.205%, 15.205%, and 15.230% for the OGMO, MGMOI, and MGMOII, respectively, in the IEEE 33 bus, 12.813%, 12.997%, and 12.997% for the OGMO, MGMOI, and MGMOII, respectively, in the IRAQI 71 bus). Finally, the proposed modified algorithms proved their superiority and dominance over the original algorithm in converging to the optimal solution for finding the optimal position and sizing of a PV-DG (after 28, 25, and 19 iterations for the OGMO, MGMOI, and MGMOII, respectively, in the IEEE 33 bus, after 27, 23, and 20 iterations for the OGMO, MGMOI, and MGMOII, respectively, in the IRAQI 71 bus), and the performance of the MGMOII is better than the performance of the MGMOI because it requires fewer iterations to reach the optimal solution.

Key words: beta probability distribution function, modified geometric mean optimizer, photovoltaic distributed generators, power losses minimized, practical Iraqi distribution networks, radial distribution networks

1. Introduction

A photovoltaic distributed generator (PV-DG) is one of the most important green energy resources that can be used to generate electricity. In recent years, interest in using PV-DGs as distribution generators in radial distribution networks (RDNs) has grown due to their numerous advantages, including reduced losses, lower fuel costs, and increased stability and reliability of RDNs. A PV-DG can be used to generate electricity in remote and rural areas far from power generation centers, where traditional electricity grids are unavailable or unreliable [1]. This study aims to investigate the impact of climate change on the performance of home photovoltaic systems and develop smart models to predict energy consumption in distributed solar plants. Combining climate analysis with data forecasting aims to improve the efficiency and sustainability of solar energy systems and support smart energy management in the face of future environmental changes [2, 3]. Furthermore, several modern algorithms have been developed to improve the performance of electrical networks that use PV-DGs as distribution generators. Optimization algorithms are used to optimize network design and determine the optimal capacity and siting for PV-DGs. The use of optimization algorithms contributes to improving network efficiency, reducing costs, and enhancing the quality and reliability of electrical power [4].

The use of PV-DGs as distribution generators in RDNs can contribute to improving network efficiency and reducing electrical losses, and help to improve the quality of electrical power and reduce environmental pollution [5, 6]. Furthermore, using PV-DGs as distribution generators can reduce greenhouse gas emission [7, 8]. Finally, it is indicated that using PV-DGs can improve grid stability and reduce the risk of power outages [9].

However, there are several challenges that must be overcome when using PV-DGs as distribution generators in RDNs, one of the main challenges is ensuring network stability and avoiding voltage and current fluctuations. This requires the development of control and monitoring techniques to ensure RDN's stability and improve its performance [10, 11]. On the other hand, PV-DG use can be affected by changes in weather and environmental conditions [12].

In the literature, many researchers have addressed modern and developed algorithms for calculating the optimal location and size of PV-DGs to improve the overall performance of RDNs. In [13], AEO-OBL (artificial ecosystem-based optimization-opposition based Learning) is an improved version of AEO utilized to compute the optimal position and capacity of a PV-DG of the RDN; the paper is comprehensive in its integration of multiple renewable energy sources. However, it suffers from limitations related to simplistic assumptions and its limited reliance on actual operating data. In [14], an improved Harris Hawks optimization (IHHO) algorithm was introduced to obtain the optimal allocation of a PV-DG to improve the performance of the RDN; the advantages of this paper include its high accuracy and speed in arriving at optimal solutions. Its drawbacks include its heavy reliance on control parameters. In [15], the authors proposed a novel student psychology-based optimization (SPBO) to obtain the optimum site and size of a PV-DG in the RDN, the paper has the potential to balance exploration and exploitation, but its limitations include only limited empirical validation and reliance on simulation studies. In [16],

the authors proposed Genetic algorithm and Teaching learning-based optimization (GA-TLBO and TLBO-GA) two newly developed schemes of optimization algorithms, to solve the optimal integration of PV-DGs and optimal network reconfiguration; the advantage of the paper is its ability to deal with complex multi-objective problems, but its disadvantages are its reliance on limited simulation environments and the lack of practical verification in real networks. In [17], a modified version of the Search Group Algorithm (SGA) was presented, named the enhanced search group algorithm (ESGA), to determine the optimal placement and capacity of PV-DGs. The paper has high efficiency in exploring the solution space and speed in reaching optimal results. It faces limitations related to the weakness of testing the algorithm in realistic operating scenarios. In [18], the multi-objective non-dominated sorting genetic algorithm II (NSGA-II) is presented to detect the optimal allocation of PV-DGs; the paper is distinguished by its comprehensive approach in integrating several evaluation criteria, but its limitations are the limited experimental verification. In [19], Rüppell's fox optimizer (RFO) is proposed to determine the optimal locations and sizes of PV-DGs in RDNs; the paper is innovative in using a new algorithm inspired by animal behavior and suffers from limitations related to poor validation in real environments. In [20], the authors introduced the AOA (arithmetic optimization algorithm) for detecting the optimal position and capacity of a PV-DG in the RDNs; the paper is distinguished by its speed in converging to the optimal solution, but its drawback is its reliance on limited simulation environments. In [21], an enhanced coyote optimization algorithm (ECOA) was implemented to optimally select the location and capacity of a PV-DG to decrease the power loss and improve voltage stability of the RDN, the paper has the ability to deal with continuous and integer variables effectively, with balanced exploration and exploitation in the solution space. Its disadvantages are the complexity of calculations and the long execution time. In [22], a modified version of homonuclear molecules optimization (mHMO) was developed to calculate the optimal allocation of a PV-DG; the paper presents an efficient integration between the PV-DG and DSTATCOM modules, which is flexible and adaptable. Its drawbacks are the difficulty of calculations and the long time to reach the solution. In [23], a multi-objective fruit fly optimization algorithm based on population Manhattan distance (pmdMOFOA) is presented to solve the optimal integration of a PV-DG in the RDN; the paper features a good diversity of solutions when using the Manhattan distance between populations and the difficulty of ensuring the global optimal solution in large and complex networks. In [24], a teaching–learning-based optimization (TLBO) was employed to solve the optimal PV-DG allocation in the RDN; the paper has the benefit of increasing system reliability and power quality and its limitation is the dependence of the results on the initial algorithm settings. In [25], an improved raven roosting optimization (IRRO) was implemented for optimal incorporating of a PV-DG in the RDN; the paper strikes a balance between the technical and economic aspects of distribution networks, and its drawback is the complexity of the calculations due to dealing with multiple objectives. In [26], a rider optimization algorithm (ROA) was employed to generate the optimal location and size of a PV-DG of the RDN; the paper has an effective integration between PV-DG units and battery energy storage (BES) units, but it has computational complexity and longer execution time due to dealing with probabilistic variables and storage constraints. In [27], an adaptive modified whale optimization algorithm (A-MWOA) was proposed to obtain the optimal allocation of PV-DGs and optimal network reconfiguration; the paper features an integrated reconfiguration solution to increase network reliability, and its drawback is that the results depend on the initial algorithm settings. In [28], the authors presented

a hybrid optimization method based on analytical and modern algorithms; the loss sensitivity factor (LSF) and sine cosine algorithm (SCA) was applied for optimal PV-DG allocation in the RDN; the paper strikes a balance between technical performance and operational cost, but is constrained by the complexity of the calculations due to the results relying on hybrid research techniques. In [29], an improved simulated annealing-based particle swarm optimization (SAPSO) was introduced for optimal incorporation of a PV-DG in the RDN; the paper features an ideal coordination between PV-DGs and electric vehicles (EVs), but its drawback is the complexity of the mathematical model due to the dynamic interaction between PV-DGs and EVs. In [30], the Mixed Particle Swarm Optimization (MPSO) was presented to identify the optimal network reconfiguration and allocation of a PV-DG in the RDN. The algorithm in this paper provides high convergence speed and accuracy in solutions, but there is an increase in computational complexity due to the combination of the PV-DG allocation and network reconfiguration stages.

Despite significant research efforts in identifying optimal locations for a PV-DG in the RDN, current challenges remain in electrical distribution networks, such as slow convergence and reliance on precise tuning criteria based on initial algorithm settings. The current research gap demonstrates the need for an efficient and effective algorithm to determine the optimal locations of a PV-DG in the RDN and reach the optimal solution with the least possible number of iterations. This paper aims to present a modified algorithm based on nonlinear optimization to achieve a balance between exploration and exploitation. The advantage of developing this algorithm is its accuracy and convergence speed, and that it can cope with the complexities of RDNs.

According to the reviewed literature, this paper proposes the use of a modified geometric mean optimizer (MGMO) to detect the optimal location and capacity of a PV-DG for its integration into the RDN. Two types of MGMOs are proposed based on the benefits of the nonlinearity of control parameters; the first is the logarithmic function (MGMOI) and the second is the exponential function (MGMOII). As a result, a balance is achieved between exploration and exploitation, using the nonlinear control parameter to reach the best optimal solution.

The major contributions of this paper are that PV-DGs are optimally sized and positioned by the proposed MGMO, as well as the optimal insertion of the PV-DGs to minimize power loss, improve voltage level and stability while maintaining the equality and inequality constraints. The main contributions of this paper are outlined as follows:

- A modified geometric mean optimizer (MGMO) is proposed to enhance the performance of the original geometric mean optimizer (OGMO).
- Assessing the validity of the proposed algorithms (MGMOI and MGMOII) compared to the original algorithm (OGMO) using benchmark functions.
- Consider the beta probability distribution function (BPDF) model as a model of the stochastic nature of PV-DGs.
- Validating the performance of the proposed algorithms (MGMOI and MGMOII) using the standard IEEE 33 bus and the practical IRAQI 71 bus distribution networks.
- Significant reduction in active and reactive power losses, significant increase in voltage level and stability when deploying a PV-DG in the RDN based on the proposed algorithms (MGMOI and MGMOII).

This paper is organized as follows: Section 2 presents the mathematical modeling of a PV-DG, and the BPDF calculation of the standard IEEE 33 bus and the practical IRAQI 71 bus distribution networks. Section 3 presents the mathematical modeling of the RDN, modeling of active and reactive

power losses, and modeling of voltage deviation and the voltage stability index. Section 4 presents the proposed algorithms (MGMOI and MGMOII) compared with the original algorithm (OGMO), using benchmark functions. Section 5 presents and discusses the simulation results based on the MGMOI and MGMOII to determine the optimal location and capacity of a PV-DG in the RDN and compare them with the OGMO. Section 6 introduced the conclusion and future work of this paper.

2. Mathematical modeling of PV-DG

Solar irradiance plays an important role in calculating the power of PV-DGs. To obtain logical solutions, it is necessary to accurately model the solar irradiance at a specific location. By analyzing historical data collected for hourly and daily solar irradiance, the mean (μ) and standard deviation (σ) are determined. The beta probability distribution function (BPDF) was applied to describe the probabilistic nature of solar irradiance over a specific time period [12, 13, 17, 25, 31, 32]. The beta distribution for solar irradiance (s) is expressed mathematically by the equation:

$$f_b(s) = \begin{cases} a & 0 \le s \le 1, \quad \alpha, \beta \ge 0 \\ 0 & \text{otherwise} \end{cases}, \tag{1}$$

$$a = \frac{\Gamma(\alpha+\beta)}{\Gamma(\alpha)\Gamma(\beta)} s^{(\alpha-1)}(1-s)^{(\beta-1)}, \tag{2}$$

where: $f_b(s)$ is the beta distribution function of s, s is the random parameter of solar radiation (kW/m^2), α and β are the factors of $f_b(s)$, which are computed using the mean (μ) and standard deviation (σ) of solar irradiance as follows:

$$\alpha = \frac{\mu * \beta}{1-\mu}, \tag{3}$$

$$\beta = (1-\mu)\left(\frac{\mu\,(1+\mu)}{\sigma^2} - 1\right). \tag{4}$$

The probability of the solar radiation state s during any given hour can be determined from Eq. (1) as follows:

$$\rho(s) = \int_{s1}^{s2} f_b(s)\mathrm{d}s, \tag{5}$$

where s_1 and s_2 are the solar irradiance limits of the state. The output power of a photovoltaic module can be modeled mathematically in any state by the equations:

$$P_{\mathrm{PV}_o}(s) = N \times \mathrm{FF} \times V_y \times I_y, \tag{6}$$

$$\mathrm{FF} = \frac{V_{\mathrm{MPP}} \times I_{\mathrm{MPP}}}{V_{OC} \times I_{SC}}, \tag{7}$$

$$V_y = V_{OC} - K_v \times T_{cy}, \tag{8}$$

$$I_y = s\left[I_{SC} + K_i \times (T_{cy} - 25)\right], \tag{9}$$

$$T_{cy} = T_A + s\left(\frac{N_{OT} - 20}{0.8}\right), \tag{10}$$

where: N represents the numbers of modules, FF is the fill factor, K_v and K_i are the temperature factors for voltage and current, respectively, T_{cy} and T_A are the cell and ambient temperatures, respectively, N_{OT} is the normal operating temperature of cell.

The total expected output power of photovoltaic module during any given period can be obtained from Eq. (5), and Eq. (5) is expressed mathematically by the equation:

$$P_{\mathrm{PV}}(t) = \int_0^t P_{\mathrm{PV_o}}(s)\,\rho(s\mathrm{d})s. \tag{11}$$

The BPDF is employed on the standard IEEE 33 buses and the practical IRAQI 71 buses (BAQ-WEST-ALRAHMA) of RDNs, based on historical data.

2.1. BPDF implemented on standard IEEE 33 buses

The IEEE 33 buses, as shown in Fig. 1, consist of 32 lines, the base voltage is 12.66 kV, the base MVA is 100 MVA. The mean (μ) and standard deviation (σ) for every hour of the day are computed by the hourly historical solar radiation data obtained hourly for a period of three years, as given in Table 1 [17, 31, 32]. The BPDF of solar irradiance are calculated for each hour of the day, for example, Fig. 2(a) and Fig. 2(b) illustrate the BPDF at 9 AM and 4 PM, respectively. Since solar irradiance changes over a 24 hour per day, therefore, the power produced by the PV-DG changes for each hour.

Table 1. Mean and standard deviation of solar radiation for IEEE 33 bus [17, 31, 32]

Hour	**6**	**7**	**8**	**9**	**10**	**11**	**12**
μ **(kW/m^2)**	0.019	0.096	0.222	0.381	0.511	0.610	0.657
σ **(kW/m^2)**	0.035	0.110	0.182	0.217	0.253	0.273	0.284
Hour	13	14	15	16	17	18	19
μ **(kW/m^2)**	0.648	0.590	0.477	0.338	0.190	0.080	0.017
σ **(kW/m^2)**	0.282	0.265	0.237	0.204	0.163	0.098	0.032

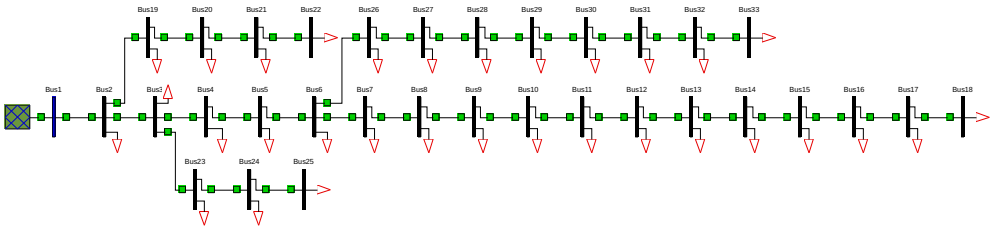

Fig. 1. One line diagram of IEEE 33 buses

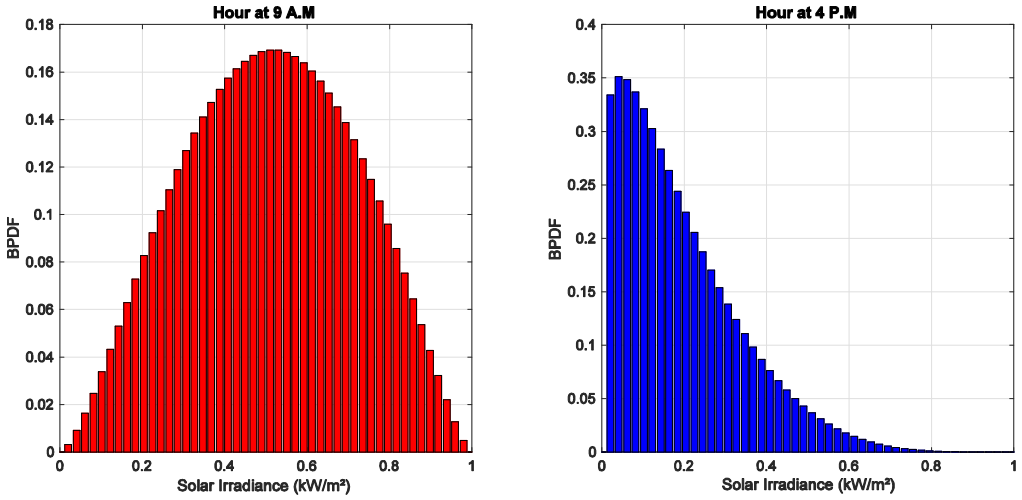

Fig. 2. BPDF of solar irradiance: (a) BPDF at 9 AM; (b) BPDF at 4 PM

2.2. BPDF implemented on practical IRAQI 71 buses

The IRAQI 71 buses (BAQ-WEST-ALRAHMA), as shown in Fig. 3, consist of 70 lines, the base voltage is 11 kV, the base MVA is 100 MVA. The mean (μ) and standard deviation (σ) for every hour of the day are computed by the hourly historical solar radiation data obtained hourly for a period of three years, as given in Table 2. The BPDF of solar radiation are calculated for each hour of the day, for example, Fig. 4(a) and Fig. 4(b) illustrate the BPDF at 7 AM and 2 PM, respectively. Since solar irradiance changes over a 24 hour per day, therefore, the power produced by the PV-DG changes for each hour.

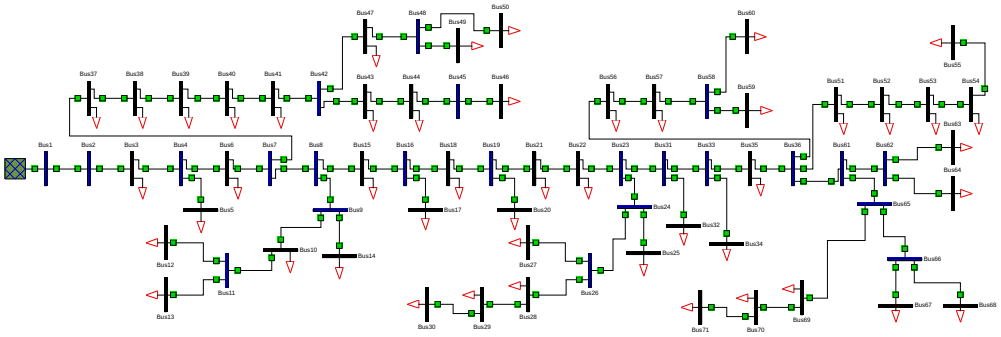

Fig. 3. One line diagram of IRAQI 71 buses

Table 2. Mean and standard deviation of solar radiation for IRAQI 71 bus

Hour	**6**	**7**	**8**	**9**	**10**	**11**	**12**
μ (kW/m^2)	0.0321	0.1661	0.3550	0.5553	0.7186	0.8430	0.9016
σ (kW/m^2)	0.0072	0.0311	0.0446	0.0395	0.0471	0.0398	0.0434
Hour	13	14	15	16	17	18	19
μ (kW/m^2)	0.9203	0.8741	0.7707	0.6104	0.4199	0.2181	0.0569
σ (kW/m^2)	0.0367	0.0373	0.0370	0.0393	0.0327	0.0241	0.0086

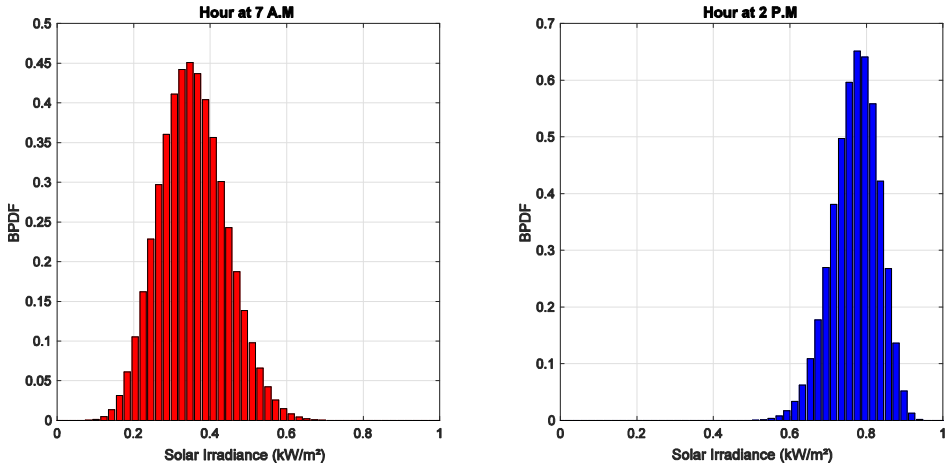

Fig. 4. BPDF of solar irradiance: (a) BPDF at 7 AM; (b) BPDF at 2 PM

3. Mathematical modeling of RDN

This part of the paper presents the mathematical modeling of the RDN, including the modeling of active power losses (APL) and reactive power losses (RPL), the modeling of the voltage deviation index (VDI) and voltage stability index (VSI), as well as equality and inequality constraints [6,7,11].

3.1. Modeling of APL and RPL

The aim is to decrease active power and reactive power losses in RDNs by incorporating PV-DGs in distribution networks. The APL and RPL modeling are mathematically expressed by the following equations:

$$\text{APL} = \sum_{i=1}^{N_B} \sum_{\substack{j=2 \\ j\neq i, j>i}}^{N_B} \left(\frac{|V_i - V_j|}{|R_{ij} + X_{ij}|} \right)^2 \times R_{ij}, \tag{12}$$

$$\mathrm{RPL} = \sum_{i=1}^{N_B} \sum_{\substack{j=2 \\ j\neq i, j>i}}^{N_B} \left(\frac{|V_i - V_j|}{|R_{ij} + X_{ij}|} \right)^2 \times X_{ij}, \tag{13}$$

where: N_B is the buses' number of the radial distribution network, V_i is the voltage at the i-th bus, V_j is the voltage at the j-th bus, R_{ij} is the resistance between the buses i-th and j-th, and X_{ij} is the reactance between the buses i-th and j-th.

3.2. Modeling of VDI and VSI

The aim is to minimize the VDI and maximize the VSI of the RDN by incorporating PV-DGs into distribution networks, the VDI and VSI modeling are mathematically expressed by the following equations:

$$\mathrm{VDI} = \left| \frac{\sum_{i=1}^{N_B} V_i}{N_B} - 1 \right|, \tag{14}$$

$$\mathrm{VSI} = \frac{1}{N_B} \sum_{i=1}^{N_B} \sum_{\substack{j=2 \\ j\neq i, j>i}}^{N_B} \left[|V_i|^4 - 4\left(P_j R_{ij} - Q_j X_{ij}\right)^2 - 4\left(P_j X_{ij} - Q_j R_{ij}\right)^2 \times |V_i|^2 \right], \tag{15}$$

where P_j is the active power at the j-th bus and Q_j is the reactive power at the j-th bus.

3.3. Equality and inequality constraints

A set of constraints (equality and inequality) must be satisfied; the active and reactive powers balanced represent equality constraints, which are mathematically expressed by the following equations:

$$P_{\mathrm{slack}} + \sum_{i=1}^{N_{\mathrm{PV}}} P_{\mathrm{PV},i} = \sum_{i=1}^{N_B} P_i^D + \mathrm{APL}, \tag{16}$$

$$Q_{\mathrm{slack}} = \sum_{i=1}^{N_B} Q_i^D + \mathrm{RPL}, \tag{17}$$

where: P_{slack} is the active power generation from the slack bus (bus 1), Q_{slack} is the reactive power generation from the slack bus (bus 1), $P_{\mathrm{PV},i}$ is the active power of the PV-DG at the i-th bus, P_i^D is the total active power demand of the RDN, Q_i^D is the total reactive power demand of the RDN.

Additionally, the voltage limits, generation of PV-DG unit limits, and PV-DG locations represent inequality constraints, which are mathematically expressed by the following equations:

$$V_i^{\min} \leq V_i \leq V_i^{\max}, \tag{18}$$

$$P_{\mathrm{PV},i}^{\min} \leq P_{\mathrm{PV},i} \leq P_{\mathrm{PV},i}^{\max}, \tag{19}$$

$$\sum_{i=1}^{N_{\mathrm{PV}}} P_{\mathrm{PV},i} \leq \sum_{i=1}^{N_B} P_i^D + \mathrm{APL}, \tag{20}$$

$$2 \leq \mathrm{PV} - \mathrm{DG}_{\mathrm{Location}} \leq N_B, \tag{21}$$

where: $V_i^{\min}$ is the minimum voltage at the i-th bus, $V_i^{\max}$ is the maximum voltage at the i-th bus, $P_{\mathrm{PV},i}^{\min}$ is the minimum active power of the PV-DG at the i-th bus, $P_{\mathrm{PV},i}^{\max}$ is the maximum active power of the PV–DG at the i-th bus, $\mathrm{PV}-\mathrm{DG}_{\mathrm{Location}}$ is the location of the PV-DG in the RDN.

4. Modified geometric mean optimizer (MGMO)

The GMO is a new optimization technique that mathematically simulates the qualitative properties of the geometric mean operator. This operator can simultaneously evaluate the objective function and the diversity of search agents in the search space. In the GMO, the weight of each agent is calculated based on the geometric mean; taking into account the corresponding measured objective values. Thus, the optimization problem can be solved based on the state of the agent to guide other agents [33–35]. To perform the GMO process mathematically, the following steps can be used in calculation:

Step 1: Calculate the fuzzy membership function (MF) for all agents using the following equation:

$$\mathrm{MF}_j^{\mathrm{iter}} = \frac{1}{1+\exp\left(-\frac{4}{\sigma^{\mathrm{iter}}\sqrt{e}}\times\left(z_{\mathrm{best},j}^{\mathrm{iter}}-\mu^{\mathrm{iter}}\right)\right)}, \quad j=1,2,\ldots,N, \tag{22}$$

where: $\mathrm{MF}_j^{\mathrm{iter}}$ is the MF value of the j-th personal best agent at the current iteration, $Z_{\mathrm{best},j}^{\mathrm{iter}}$ is the fitness function amount of the j-th personal best agent at the current iteration, σ^{iter} and μ^{iter} are the standard and mean deviations of the fitness function amount of all agents at the current iteration.

Step 2: Calculate the dual fitness index (DFI) for a search agent using the following equation:

$$\mathrm{DFI}_i^{\mathrm{iter}} = \mathrm{MF}_1^{\mathrm{iter}}\times\ldots\times\mathrm{MF}_{i-1}^{\mathrm{iter}} * \mathrm{MF}_{i+1}^{\mathrm{iter}}\times\ldots\times\mathrm{MF}_N^{\mathrm{iter}} = \prod_{\substack{j=1\\ j\neq i}}^{N}\mathrm{MF}_j^{\mathrm{iter}}, \tag{23}$$

where $\mathrm{DFI}_i^{\mathrm{iter}}$ is the DFI of the i-th agent at the current iteration, and N is the number of the population.

Step 3: Calculate the locations of guide agents using the following equation:

$$Y_i^{\mathrm{iter}} = \frac{\sum_{j\in N\mathrm{best},j\neq i}\mathrm{DFI}_j^{\mathrm{iter}}\times X_j^{\mathrm{best}}}{\sum_{j\in N\mathrm{best}}\mathrm{DFI}_j^{\mathrm{iter}}+\varepsilon}, \tag{24}$$

where: Y_i^{iter} is the location parameter of the unique global directory agent computed for the agent i-th at the current iteration, X_j^{best} is the best location parameter of the j-th search agent, ε is a very small positive number to prevent singularity.

Step 4: The Gaussian mutation process is incorporated to grow the diversity of the guide agents. This mutation process is expressed using the following equation:

$$Y_{i,\mathrm{mut}}^{\mathrm{iter}} = Y_i^{\mathrm{iter}} + w * \mathrm{rand}\, n\times\left(\mathrm{Std}_{\max}^{\mathrm{iter}}-\mathrm{Std}^{\mathrm{iter}}\right), \tag{25}$$

where: $Y_{i,\text{mut}}^{\text{iter}}$ represents the mutated Y_i^{iter} used for guide search agents at the current iteration, rand n represents a random number derived from the standard normal distribution, $\text{Std}_{\text{max}}^{\text{iter}}$ represents the maximum standard deviation value of the best agents at the current iteration, Std^{iter} represents the standard deviation parameter computed for the best agents at the current iteration, and w is the control parameter used to keep balance between exploration and exploitation when searching for optimal solutions and described briefly in Section 4.1.

Step 5: The update velocity and location of the agents are expressed using the following equations:

$$V_i^{\text{iter}+1} = w \times V_i^{\text{iter}} + \varphi \times \left(Y_{i,\text{mut}}^{\text{iter}} - X_i^{\text{iter}}\right), \tag{26}$$

$$X_i^{\text{iter}+1} = X_i^{\text{iter}} + V_i^{\text{iter}+1}, \tag{27}$$

$$\varphi = 1 + (2 \times \text{rand} - 1) \times w, \tag{28}$$

where: $V_i^{\text{iter}+1}$ is the velocity of the i-th agent at the (iter + 1) iteration, V_i^{iter} is the velocity of the i-th agent at the current iteration, $X_i^{\text{iter}+1}$ is the location of the i-th agent at the (iter + 1) iteration, X_i^{iter} is the location of the i-th agent at the current iteration, φ is the scaling parameter vector, rand is the random coefficient number that lies between 0 and 1.

4.1. Control parameter (w)

The control parameter (w) mentioned in Eq. (25), Eq. (26), and Eq. (28) decreases linearly in the original geometric mean optimizer (OGMO). This leads to an imbalance between exploration and exploitation when searching for optimal solutions within the search region. Therefore, the search process does not cover the entire region, and the chance of the agents converging to the optimal solution quickly is slow. To overcome this problem, an improvement on the control parameter (w) is proposed where it decreases nonlinearly. Consequently, the optimal solution can be converged more quickly.

In the OGMO, the control parameter (w) is expressed by the equation:

$$w = 1 - \frac{\text{iter}}{\max \text{iter}}. \tag{29}$$

Two formulas, a logarithmic function MGMOI and exponential function MGMOI were proposed in the modified geometric mean optimizer (MGMO). They are expressed mathematically using the following equations:

$$w = \log_2 \left[1 + \left(-\frac{\text{iter}}{\max \text{iter}}\right)^3\right], \tag{30}$$

$$w = \exp^{\left(-2.5 \times \left(\frac{\text{iter}}{\max \text{iter}}\right)\right)^2}. \tag{31}$$

According to Eqs. (29), (30), and (31), Fig. 5 shows the behavior of the control parameter (w) with iterations. The rate of change is observed to be constant for the OGMO; making it suitable for early convergence toward local optimum values. Therefore, we propose a nonlinear control parameter (MGMOI and MGMOII) to improve the global search. The nonlinear control parameter

(MGMOI and MGMOII) changes rapidly, which enhances the overall search ability, improves the search range efficiency, accelerates the convergence speed, and improves the flexibility of detecting optimal solutions.

To verify the validity and effectiveness of the proposed control parameter, the MGMOI and MGMOII were implemented and compared with the OGMO based on benchmark functions in the next part of the paper.

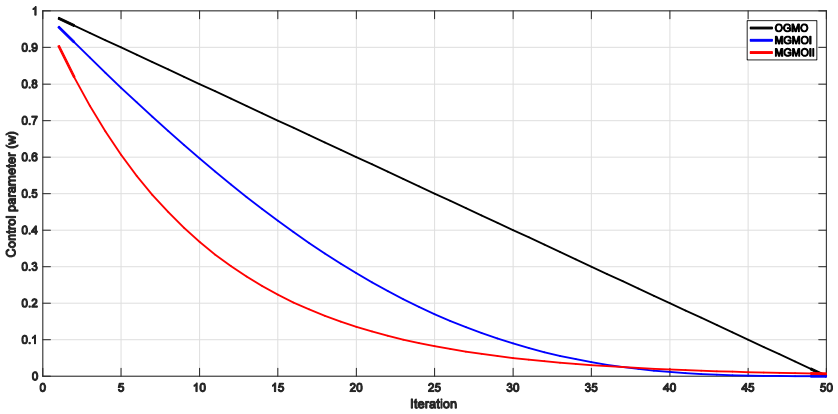

Fig. 5. The control parameter (w) verse iterations

4.2. Validation of MGMO based on benchmark functions

To verify the validity, accuracy, effectiveness, and performance of the proposed modified algorithms, the MGMOI and MGMOII were applied to 5 benchmark functions and compared with the original algorithm (OGMO). The benchmark functions are expressed mathematically by the fo llowing equations:

$$y_1 = \max_i \{|x_i|, 1 \le i \le d\}, \tag{32}$$

$$y_2 = \sum_{i=1}^{d} \left[x_i^2 - 10\cos(2\pi x_i) + 10\right], \tag{33}$$

$$y_3 = \frac{1}{4000}\sum_{i=1}^{d} x_i^2 - \prod_{i=1}^{d} \cos\left(\frac{x_i}{\sqrt{i}}\right) + 1, \tag{34}$$

$$y_4 = 4x_1^2 - 2.1x_1^4 + \frac{1}{3}x_1^6 + x_1x_2 - 4x_2^2 + 4x_2^4, \tag{35}$$

$$y_5 = -\sum_{i=1}^{5} \left[(X - a_i)(X - a_i)^T + c_i\right]^{-1}, \tag{36}$$

where: y_1 represents the unimodal benchmark function, y_2 and y_3 represent the multimodal benchmark functions, while y_4 and y_5 represent the fixed-dimension multimodal benchmark functions [16, 36].

The statistical performance represented by the average (mean), standard deviation (std), best and execution time was presented in Table 3. The results were obtained from 20 runs, a maximum iteration of 50, and a population of 50. The specifications of the personal computer are: Intel(R) Core(TM) i5-7200U CPU @2.50Gz, Installed RAM 4.00 GB.

Table 3. The statistical performance of the benchmark functions

		Mean	Std	Best	Time
y_1	**OGMO**	1.9842e-12	6.0191e-12	4.3521e-13	7.7332
	MGMOI	2.8891e-31	9.6687e-31	1.1563e-31	7.7005
	MGMOII	7.3363e-32	2.3204e-32	3.3462e-33	7.6836
y_2	**OGMO**	22.2365	39.0695	0.000	7.7302
	MGMOI	7.1739	26.6196	0.000	7.6648
	MGMOII	5.7727	25.8164	0.000	7.6269
y_3	**OGMO**	9.7235e-07	4.3485e-06	0.000	8.1201
	MGMOI	6.2741e-13	5.5382e-13	0.000	8.0761
	MGMOII	4.9693e-22	8.6603e-21	0.000	7.8127
y_4	**OGMO**	–1.0297	4.6227e-03	–1.0316	6.9766
	MGMOI	–1.0309	1.7207e-03	–1.0316	6.9178
	MGMOII	–1.0519	1.0766e-05	–1.0316	6.8792
y_5	**OGMO**	–8.1411	3.2216	–10.1532	7.9344
	MGMOI	–8.4309	3.1659	–10.1532	7.8634
	MGMOII	–9.2715	2.2017	–10.1532	7.7789

Figures 6(a), 7(a), 8(a), 9(a), and 10(a) illustrate the convergence rates of the proposed algorithms. Consequently, by carefully observing the shape of the curves, it is clear that the MGMOII converges to the best solution faster and with less iteration compared to the MGMOI and OGMO. Moreover, the MGMOI converges to the best solution faster and with fewer iterations compared to the OGMO.

In addition to the convergence rates, the results were represented using box plots to visually depict the distribution of the data in the quartiles. The box plot curves were presented in Figs. 6(b), 7(b), 8(b), 9(b), and 10(b), where the MGMOII achieved the best distribution and lowest mean line values compared to the MGMOI and OGMO. Furthermore, the MGMOI achieved the best distribution and lowest mean line values compared to the OGMO.

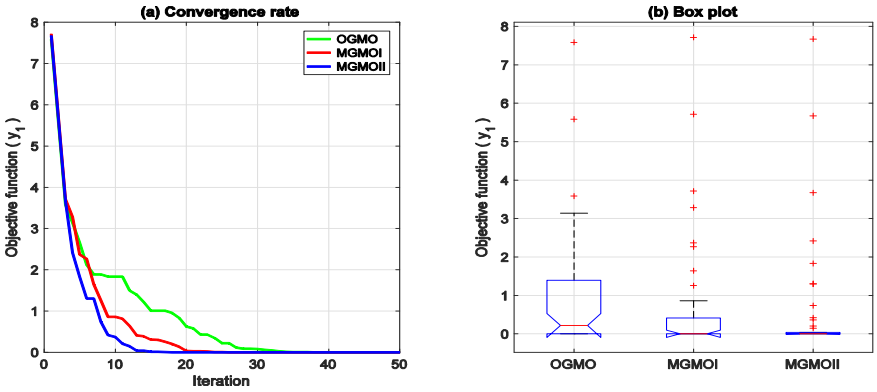

Fig. 6. OGMO and MGMO performance of y_1: (a) convergence rate; (b) box plot

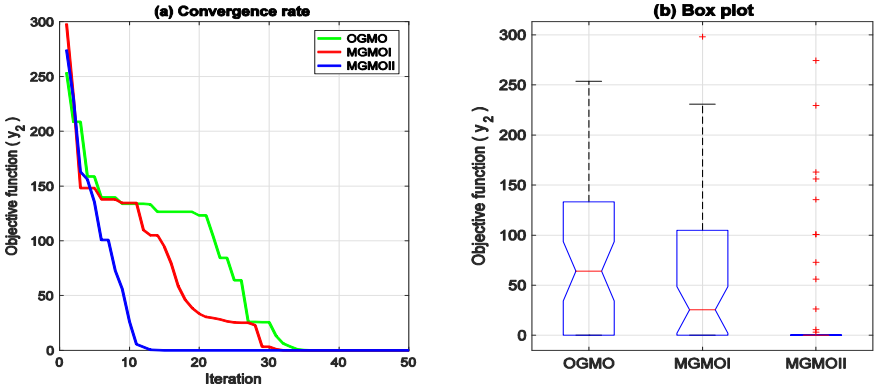

Fig. 7. OGMO and MGMO performance of y_2: (a) convergence rate; (b) box plot

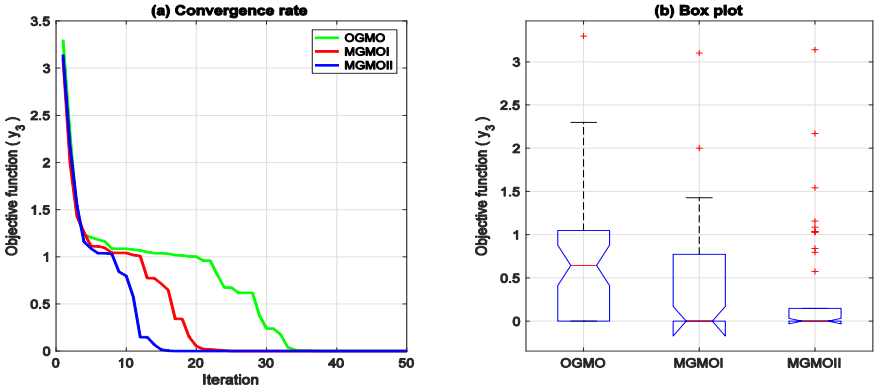

Fig. 8. OGMO and MGMO performance of y_3: (a) convergence rate; (b) box plot

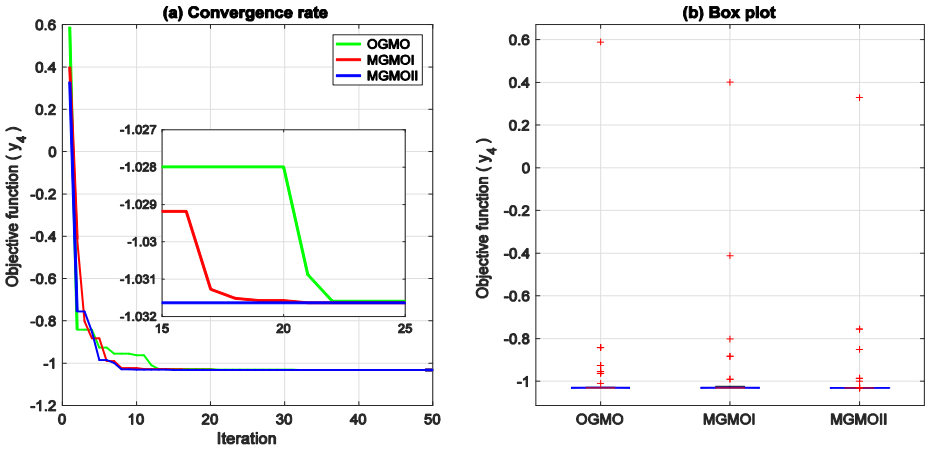

Fig. 9. OGMO and MGMO performance of y_4: (a) convergence rate; (b) box plot

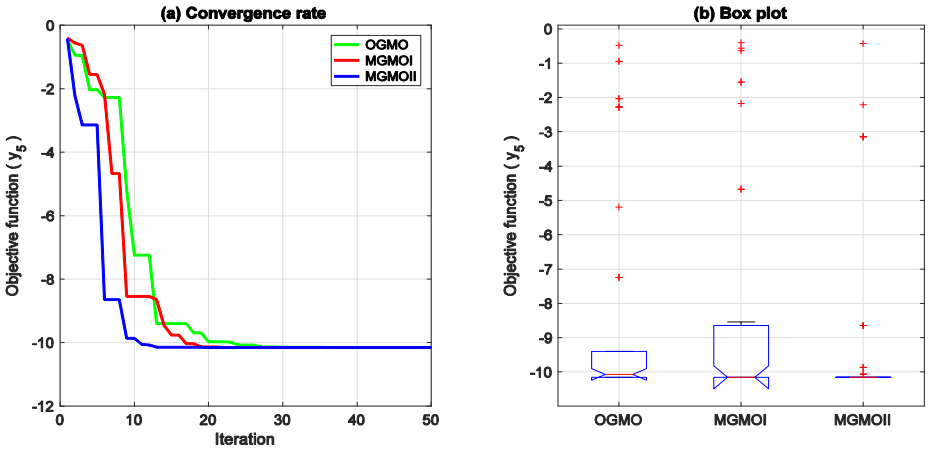

Fig. 10. OGMO and MGMO performance of y_5: (a) convergence rate; (b) box plot

5. Simulation results and discussion

A MGMO is implemented on the standard IEEE 33 bus RDN and on the practical IRAQI 71 bus (BAQ-WEST-ALRAHMA) RDN; the validation of the MGMOI and MGMOII to compute the optimal position and sizing of the PV-DG is satisfied compared with the OGMO. The flowchart for detecting the optimal allocation of the PV-DG in the RDN using the OGMO, MGMOI, and MGMOII is shown in Fig. 11, and the pseudo-code algorithm has been shown in Fig. 12. The results of load flow analysis are carried out using the backward-foreword sweep algorithm.

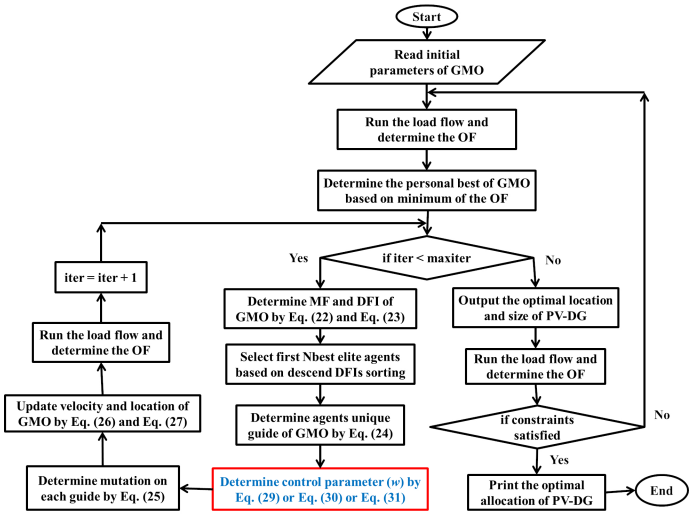

Fig. 11. Flowchart of the proposed MGMO to detect the optimal allocation of PV-DG

Algorithm GMO for Optimal PV-DG Allocation

Initialize parameters: population size N, MaxIter, ...etc
Initialize population X[i], i = 1 to N within bounds
Run LoadFlow(X[i]) to determine OF[i]
Determine Personal Best Pbest[i] = X[i] if OF[i] is minimum
iter = 1
while iter ≤ MaxIter do
  Compute MF[i] and DFI[i] using Eq. (22) and (23)
  Sort agents by DFI in descending order
  Select top Nbest elite agents
  For each agent i:
    Determine unique guide G[i] using Eq. (24)
    Determine control parameter w using Eq. (29) or (30) or (31)
    Apply mutation on G[i] using Eq. (25)
    Update velocity and location using Eq. (26) and (27)
  Run LoadFlow(X[i]) and determine new OF[i]
  If OF[i] < Pbest[i] then
    Pbest[i] = X[i]
  iter = iter + 1
end while
If constraints satisfied: Output the optimal location and size of PV-DG
Print results: Optimal PV-DG Allocation Found
End Algorithm

Fig. 12. Algorithm GMO for optimal PV-DG allocation

5.1. Results of IEEE 33 buses RDN

The one-line diagram of the IEEE 33 bus is presented in Fig. 1; it consists of 32 lines, the base voltage is 12.66 kV, the base MVA is 100 MVA, the total active power load is 3 715 kW, and the total reactive power load is 2300 kvar [37]. The base case power flow results are as follows: The APL is 210.99 kW, the RPL is 143.03 kvar, the VDI is 0.0547 per unit, and the VSI is 0.8043 per unit.

The proposed algorithms were implemented to determine the three optimal PV-DG sizes and locations when the APL is considered as an objective function (OF). From the results presented in Table 4, we observed an improvement in the overall performance of the RDN compared to the baseline case. From the convergence rate curves illustrated in Fig. 13(a), it is observed that the proposed algorithms accelerated and converged to the optimal solution are in the following order: the MGMOII is ranked first, the MGMOI is ranked second, and the OGMO is ranked last. Furthermore, Fig. 13(b) illustrates the box plot behavior of the proposed algorithms, and it is observed that some of them outperform and dominate each other in the following order: the MGMOII ranks first, the MGMOI ranks second, and the OGMO ranks last.

Table 4. Results of PV-DG for IEEE 33 buses

	PV location	**PV size (kW)**	**APL (kW)**	**RPL (kvar)**	**VDI (P.U)**	**VSI (P.U)**
OGMO	13, 25, 30	821.3, 883.5, 1069.4	73.51	50.99	0.0190	0.9266
MGMOI	14, 24, 30	769.7, 1096.2, 1067.4	72.79	50.69	0.0191	0.9266
MGMOII	14, 24, 30	800.8, 1092.6, 1054.3	72.78	50.65	0.0190	0.9268

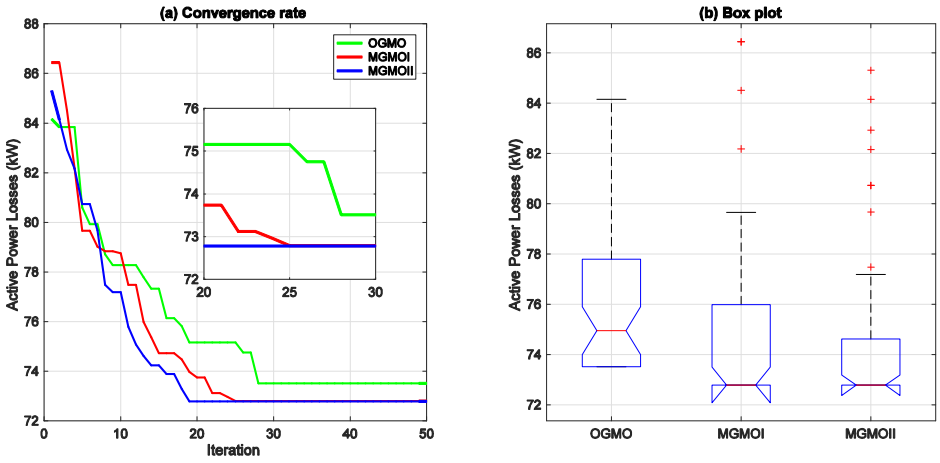

Fig. 13. OGMO and MGMO performance of IEEE 33 bus: (a) convergence rate; (b) box plot

On the other hand, the overall performance of the RDN is enhanced after incorporated the PV-DG; the reductions of active power losses are 65.159%, 65.500%, and 65.505% for the OGMO, MGMOI, and MGMOII, respectively. The reductions of reactive power losses are 64.350%, 64.559%, and 64.587% for the OGMO, MGMOI, and MGMOII, respectively, and the voltage profile is shown in Fig. 14.

Moreover, the power produced by the PV-DG changes each hour. Figure 15(a) shows the active power of three PV-DG positions on buses 13, 25, and 30 for the OGMO. Figure 15(b) shows the active power of three PV-DG positions on buses 14, 24, and 30 for the MGMOI, and Fig. 15(c) shows the active power of three PV-DG positions on buses 14, 24, and 30 for the MGMOII. The

power curves shown in Fig. 15 follow a realistic and regular physical pattern that reflects the natural variation in solar radiation throughout the day, without any anomalous behavior or inflated model output. This confirms that the proposed model was not overly tuned to specific data, but rather demonstrated stable and consistent performance at different points on the grid and under a variety of conditions, enhancing its generalizability and reducing the risk of overfitting.

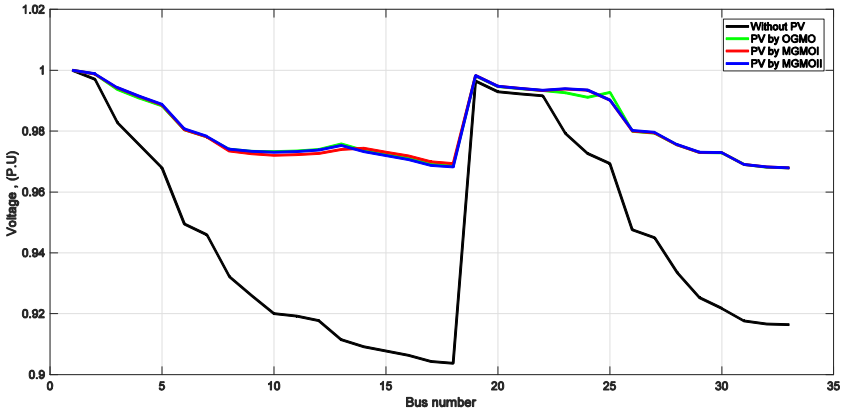

Fig. 14. The voltage profile of IEEE 33 bus

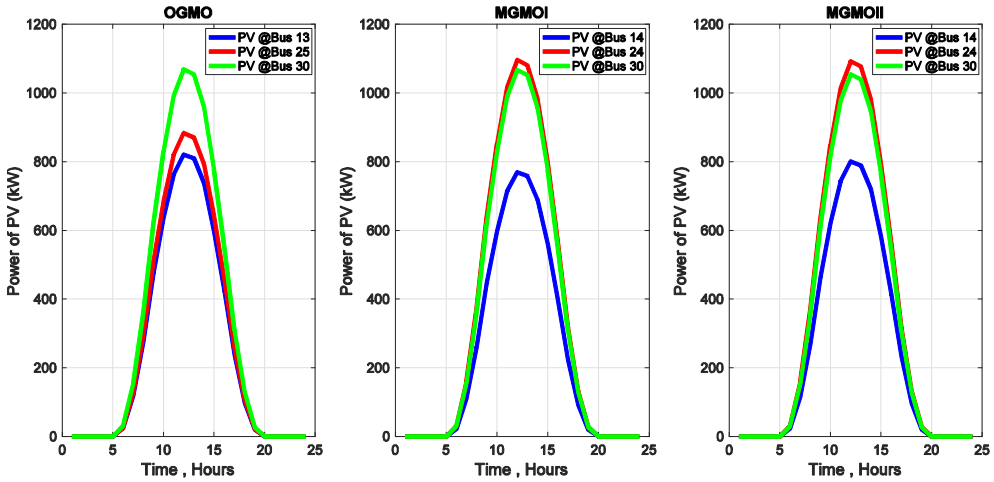

Fig. 15. PV output power of IEEE 33 bus: (a) PV by OGMO; (b) PV by MGMOI; (c) PV by MGMOII

5.2. Results of IRAQI 71buses RDN

The one-line diagram of the IRAQI 71 bus (BAQ-WEST-ALRAHMA) is presented in Fig. 3; it consists of 70 lines, the base voltage is 11 kV, the base MVA is 100 MVA, the total active power load is 8956 kW and the total reactive power load is 5542 kvar. The base case power flow results are as follows: the APL is 532.95 kW, the RPL is 650.51 kvar, the VDI is 0.0674 per unit, and the VSI is 0.7586 per unit.

The proposed algorithms were implemented to determine the three optimal PV-DG sizes and locations when the APL is considered as an objective function (OF). From the results presented in Table 5, we observed an improvement in the overall performance of the RDN compared to the baseline case. From the convergence rate curves illustrated in Fig. 16(a), it is observed that the proposed algorithms are accelerated and converged to the optimal solution in the following order: the MGMOII is ranked first, the MGMOI is ranked second, and the OGMO is ranked last. Furthermore, Fig. 16(b) illustrates the box plot behavior of the proposed algorithms, and it is observed that some of them outperform and dominate each other in the following order: the MGMOII ranks first, the MGMOI ranks second, and the OGMO ranks last.

Table 5. Results of PV-DG for IRAQI 71 buses

	PV location	PV size (kW)	APL (kW)	RPL (kvar)	VDI (P.U)	VSI (P.U)
OGMO	8, 34, 67	1972.4, 2398.6, 1781.7	177.26	216.38	0.0383	0.8558
MGMOI	11, 35, 66	1941.3, 2404.8, 1758.5	176.63	215.60	0.0379	0.8572
MGMOII	11, 36, 65	1927.6, 2407.2, 1767.4	173.26	211.46	0.0379	0.8572

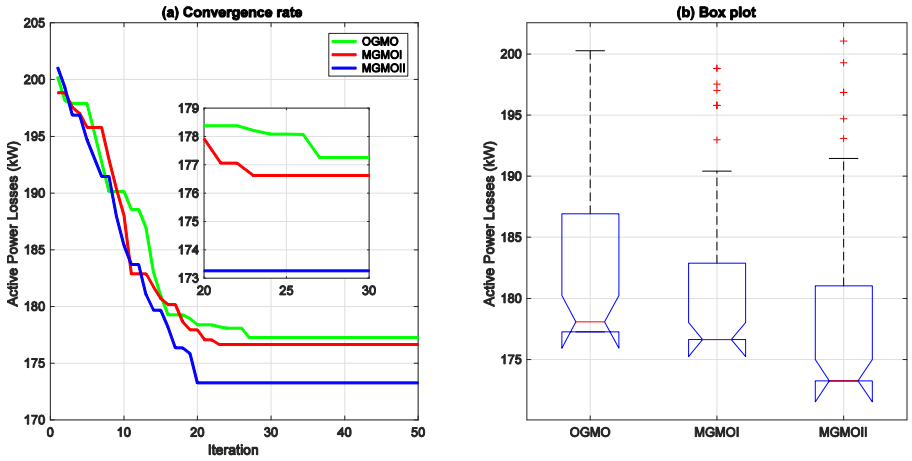

Fig. 16. OGMO and MGMO performance of IRAQI 71 bus: (a) onvergence rate; (b) box plotc

On the other hand, the overall performance of the RDN is enhanced after the PV-DG is incorporated; the reductions of active power losses are 66.739%, 66.858%, and 67.490% for the OGMO, MGMOI, and MGMOII, respectively. The reductions of reactive power losses are 66.736%, 66.856%, and 67.493% for the OGMO, MGMOI, and MGMOII, respectively, and the voltage profile is shown in Fig. 17.

Moreover, the power produced by the PV-DG changes each hour. Figure 18(a) shows the active power of three PV-DG positions on buses 8, 34, and 67 for the OGMO. Figure 18(b) shows the active power of three PV-DG positions on buses 11, 35, and 66 for the MGMOI, and Fig. 18(c) shows the active power of three PV-DG positions on buses 11, 36, and 65 for the

MGMOII. Figure 18 illustrates that the behavior of the generated power follows a realistic physical pattern that reflects the variation in solar radiation throughout the day, without any illogical fluctuations or exaggeration in the resulting values. A clear gradient is also evident between different node locations, consistent with local radiation levels in the network. These results indicate that the proposed model maintained stable performance and accuracy across various locations and operating conditions, confirming its adaptability and robustness against overfitting.

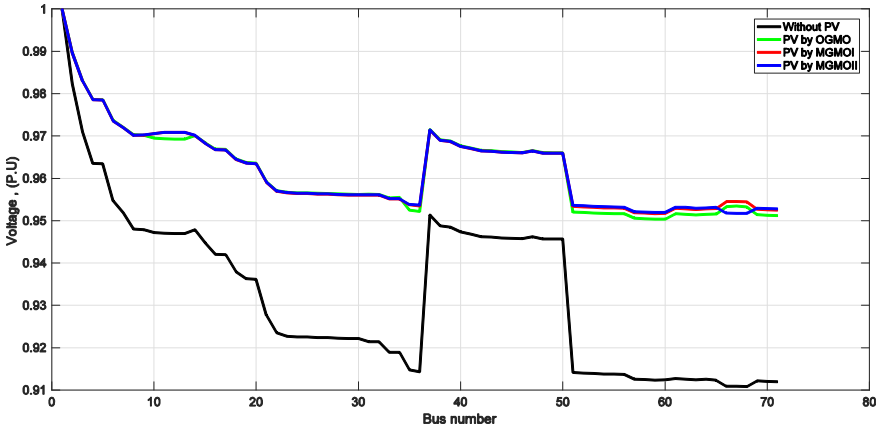

Fig. 17. The voltage profile of IRAQI 71 bus

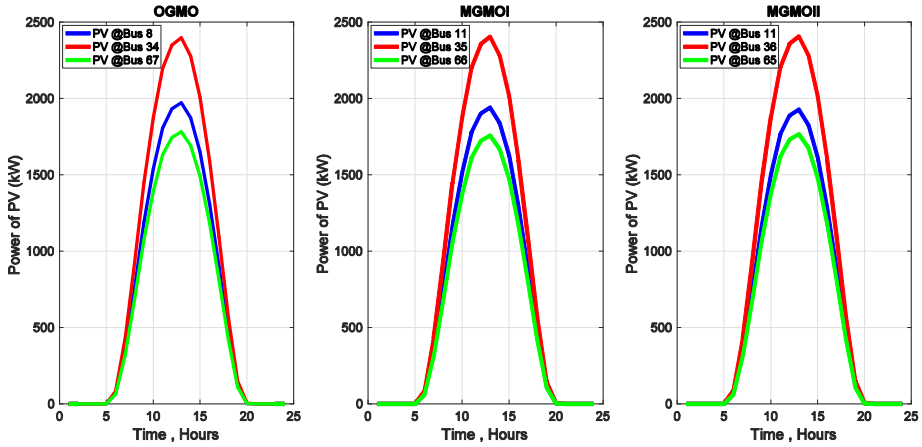

Fig. 18. PV output power of IRAQI 71 bus: (a) PV by OGMO; (b) PV by MGMOI; (c) PV by MGMOII

6. Conclusions

This paper presents two modified versions of the original geometric mean optimizer (OGMO) by modifying the linear control parameter and converting it to a nonlinear control parameter using a logarithmic function as the first modification (MGMOI) and using an exponential function as

the second modification (MGMOII). The proposed algorithms (OGMO, MGMOI, and MGMOII) have been validated and proven effective by performing quantification on benchmark functions. In addition, the proposed algorithms were used to calculate the optimal values and optimal locations of a PV-DG on the standard IEEE 33 bus and the practical IRAQI 71 bus. Regarding the uncertainty in solar irradiation intensity, mathematical modeling was performed using the beta probability distribution function (BPDF). The simulation results showed a significant enhancement in the performance of both the standard RDN and practical RDN after incorporating a PV-DG in the networks, which led to a diminution in both active power losses (APL) and reactive power losses (RPL). The results also showed that the voltage stability index (VSI) was maximized, and the level of the voltage profile for each bus has reached a level higher than the minimum allowable limit (VDI is minimized). Moreover, comparing the proposed algorithms to find optimal solutions based on convergence rate curves and box plot curves shows the dominance and precedence of the proposed algorithms according to the following order: the MGMOII is ranked first (reduction RPL is 67.493% for IRAQI 71 bus), the MGMOI is ranked second (reduction RPL is 66.856% for IRAQI 71 bus), and the OGMO is ranked last (reduction RPL is 66.736% for IRAQI 71 bus). This article can be highlighted in the future work by enhancing network resilience and the impact of a PV-DG on the resilience of the RDN in the event of earthquakes, typhoons, or strong winds. Furthermore, the proposed algorithms can be used to improve energy management by integrating energy storage systems (EESs) and electric vehicles (EVs) into the model to manage charging and discharging.

References

[1] Nguyen T.X., Lis R., *Optimal size and location of dispatchable distributed generators in an autonomous microgrid using Honey Badger algorithm*, Archives of Electrical Engineering, vol. 72, no. 4, pp. 871–893 (2023), DOI: 10.24425/aee.2023.147416.

[2] Yao J.F., Xiao C., Hao J.B., Yang X., *Research on Power Consumption Data Prediction of Distributed Photovoltaic Power Station*, HighTech and Innovation Journal, vol. 5, no. 4, pp. 937–948 (2024), DOI: 10.28991/HIJ-2024-05-04-05.

[3] Bozsik N., Szeberényi A., *Impact of climate change on the performance of household-scale photovoltaic systems*, HighTech and Innovation Journal, vol. 5, no. 1, pp. 1–15 (2024), DOI: 10.28991/HIJ-2024-05-01-01.

[4] Liu H., Qu J., Yang S., Li Y., *Intelligent optimal dispatching of active distribution network using modified flower pollination algorithm*, Archives of Electrical Engineering, vol. 69, no. 1, pp. 159–174 (2020), DOI: 10.24425/aee.2020.131765.

[5] Ufa R.A., Malkova Y.Y., Rudnik V.E., Andreev M.V., Borisov V.A., *A review on distributed generation impacts on electric power system*, International journal of hydrogen energy, vol. 47, no. 47, pp. 20347–20361 (2022), DOI: 10.1016/j.ijhydene.2022.04.142.

[6] Gao H., Diao R., Zhong Y., Zeng R., Wu Q., Jin S., *Optimal allocation of distributed generation in active distribution power network considering HELM-based stability index*, International Journal of Electrical Power & Energy Systems, vol. 155, 109508 (2024), DOI: 10.1016/j.ijepes.2023.109508.

[7] Salimon S.A., Fajinmi I.O., Adewuyi O.B., Pandey A.K., Adebiyi O.W., Kotb H., *Graph theory-enhanced integrated distribution network reconfiguration and distributed generation planning: A comparative techno-economic and environmental impacts analysis*, Cleaner Engineering and Technology, vol. 22, 100808 (2024), DOI: 10.1016/j.clet.2024.100808.

[8] Anitha M., Kotaiah N.C., Rajesh Patil, Nagaraja Kumari C.H., *White Shark Optimizer for Multi-Objective Optimal Allocation of Photovoltaic Distribution Generation in Electrical Distribution Networks Considering Different Kinds of Load Models and Penetration Levels*, International Journal of Intelligent Engineering & Systems, vol. 15, no. 4 (2022), DOI: 10.22266/ijies2022.0831.41.

[9] Jadoun V., *Risk-based dynamic pricing by metaheuristic optimization approach for electric vehicle charging infrastructure powered by grid integrated microgrid system*, Electric Power Systems Research, vol. 230, 110250 (2024), DOI: 10.1016/j.epsr.2024.110250.

[10] Luo F., Bu Q., Ye Z., Yuan Y., Gao L., Lv P., *Dynamic reconstruction strategy of distribution network based on uncertainty modeling and impact analysis of wind and photovoltaic power*, IEEE Access, vol. 12, pp. 64069–64078 (2024), DOI: 10.1109/ACCESS.2024.3394856.

[11] Alyu A.B., Salau A.O., Khan B., Eneh J.N., *Hybrid GWO-PSO based optimal placement and sizing of multiple PV-DG units for power loss reduction and voltage profile improvement*, Scientific Reports, vol. 13, no. 1, 6903 (2023), DOI: 10.1038/s41598-023-34057-3.

[12] Merlin Sajini M.L., Suja S., Merlin Gilbert Raj S., *Impact analysis of time-varying voltage-dependent load models on hybrid DG planning in a radial distribution system using analytical approach*, IET Renewable Power Generation, vol. 15, no. 1, pp. 153–172 (2021), DOI: 10.1049/rpg2.12013.

[13] Khasanov M., Kamel S., Halim Houssein E., Rahmann C., Hashim F.A., *Optimal allocation strategy of photovoltaic-and wind turbine-based distributed generation units in radial distribution networks considering uncertainty*, Neural Computing and Applications, vol. 35, no. 3, pp. 2883–2908 (2023), DOI: 10.1007/s00521-022-07715-2.

[14] Selim A., Kamel S., Alghamdi A.S., Jurado F., *Optimal placement of DGs in distribution system using an improved Harris hawks optimizer based on single-and multi-objective approaches*, IEEE Access, vol. 8, pp. 52815–52829 (2020), DOI: 10.1109/ACCESS.2020.2980245.

[15] Balu K., Mukherjee V., *Optimal siting and sizing of distributed generation in radial distribution system using a novel student psychology-based optimization algorithm*, Neural Computing and Applications, vol. 33, no. 22, pp. 15639–15667 (2021), DOI: 10.1007/s00521-021-06185-2.

[16] Iftikhar M.Z., Imran K., *Network reconfiguration and integration of distributed energy resources in distribution network by novel optimization techniques*, Energy Reports, vol. 12, pp. 3155–3179 (2024), DOI: 10.1016/j.egyr.2024.08.067.

[17] Huy T.H.B., Vo D.N., Truong K.H., Van Tran T., *Optimal distributed generation placement in radial distribution networks using enhanced search group algorithm*, IEEE Access, vol. 11, pp. 103288–103305 (2023), DOI: 10.1109/ACCESS.2023.3316725.

[18] Khoshayand H.A., Wattanapongsakorn N., Mahdavian M., Ganji E., *A new method of decision making in multi-objective optimal placement and sizing of distributed generators in the smart grid*, Archives of Electrical Engineering, vol. 72, no. 1, pp. 253–271 (2023), DOI: 10.24425/aee.2023.143700.

[19] Bouali Y., Alamri B., *Enhancing Radial Distribution System Performance Through Optimal Allocation and Sizing of Photovoltaic and Wind Turbine Distribution Generation Units with Rüppell's Fox Optimizer*, Mathematics, vol. 13, no. 15, 2399 (2025), DOI: 10.3390/math13152399.

[20] Pamuk N., Uzun U.E., *Optimal allocation of distributed generations and capacitor banks in distribution systems using arithmetic optimization algorithm*, Applied Sciences, vol. 14, no. 2, 831 (2024), DOI: 10.3390/app14020831.

[21] Pham T.D., Nguyen T.T., Dinh B.H., *Find optimal capacity and location of distributed generation units in radial distribution networks by using enhanced coyote optimization algorithm*, Neural Computing and Applications, vol. 33, no. 99, pp. 4343–4371 (2021), DOI: 10.1007/s00521-020-05239-1.

[22] Belbachir N., Kamel S., Hashim F.A., Yu J., Zeinoddini-Meymand H., Sabbeh S.F., *Optimizing the hybrid PVDG and DSTATCOM integration in electrical distribution systems based on a modified homonuclear molecules optimization algorithm*, IET Renewable Power Generation, vol. 17, no. 12, pp. 3075–3096 (2023), DOI: 10.1049/rpg2.12826.

[23] Tang M., Zhang K., Wang Q., Cheng H., Yang S., Du H., *Application of multi-objective fruit fly optimisation algorithm based on population Manhattan distance in distribution network reconfiguration*, Archives of Electrical Engineering, vol. 70, no. 2, pp. 307–323 (2021), DOI: 10.24425/aee.2021.136986.

[24] Ebrahimi A., Moradlou M., Bigdeli M., Mashhadi M.R., *Optimal sizing and allocation of PV-DG and DSTATCOM in the distribution network with uncertainty in consumption and generation*, Discover Applied Sciences, vol. 7, no. 5, 411 (2025), DOI: 10.1007/s42452-025-06870-0.

[25] Nagaballi S., Kale V.S., *Pareto optimality and game theory approach for optimal deployment of DG in radial distribution system to improve techno-economic benefits*, Applied Soft Computing, vol. 92, 106234 (2020), DOI: 10.1016/j.asoc.2020.106234.

[26] Khasanov M., Kamel S., Rahmann C., Hasanien H.M., Al-Durra A., *Optimal distributed generation and battery energy storage units integration in distribution systems considering power generation uncertainty*, IET Generation, Transmission & Distribution, vol. 15, no. 24, pp. 3400–3422 (2021), DOI: 10.1049/gtd2.12230.

[27] Uniyal A., Sarangi S., *Optimal network reconfiguration and DG allocation using adaptive modified whale optimization algorithm considering probabilistic load flow*, Electric Power Systems Research, vol. 92, 106909 (2021), DOI: 10.1016/j.epsr.2020.106909.

[28] Selim A., Kamel S., Mohamed A.A., Elattar E.E., *Optimal allocation of multiple types of distributed generations in radial distribution systems using a hybrid technique*, Sustainability, vol. 13, no. 12, 6644 (2021), DOI: 10.3390/su13126644.

[29] Tang H., Wu J., *Multi-objective coordination optimisation method for DGs and EVs in distribution networks*, Archives of Electrical Engineering, vol. 68, no. 1, pp. 15–32 (2019), DOI: 10.24425/aee.2019.125977.

[30] Essallah S., Khedher A., *Optimization of distribution system operation by network reconfiguration and DG integration using MPSO algorithm*, Renewable Energy Focus, vol. 34, pp. 37–46 (2020), DOI: 10.1016/j.ref.2020.04.002.

[31] Hung D.Q., Mithulananthan N., Lee K.Y., *Determining PV penetration for distribution systems with time-varying load models*, IEEE Transactions on Power Systems, vol. 29, no. 6, pp. 3048–3057 (2014), DOI: 10.1109/TPWRS.2014.2314133.

[32] Hung D.Q., Mithulananthan N., Bansal R.C., *Integration of PV and BES units in commercial distribution systems considering energy loss and voltage stability*, Applied Energy, vol. 113, pp. 1162–1170 (2014), DOI: 10.1016/j.apenergy.2013.08.069.

[33] Rezaei F., Safavi H.R., Abd Elaziz M., Mirjalili S., *GMO: geometric mean optimizer for solving engineering problems*, Soft Computing, vol. 27, no. 15, pp. 10571–10606 (2023), DOI: 10.1016/j.eswa.2017.07.043.

[34] Xin S., Jiahao L., Yujun Y., Jianlin T., Xiaoming L., Bin Q., *Bi-level optimal dispatching of distribution network considering friendly interaction with electric vehicle aggregators*, Frontiers in Energy Research, vol. 11, 1338807 (2023), DOI: 10.3389/fenrg.2023.1338807.

[35] Jaiswal D., Mittal M., Mittal V., *Improving the performance of grid connected PV system with dynamic voltage restorer using geometric mean optimization*, Engineering Research Express, vol. 7, no. 2, 025318 (2025), DOI: 10.1088/2631-8695/adc972.

[36] Li Y., Geng Y., Sheng H., *An improved mountain gazelle optimizer based on chaotic map and spiral disturbance for medical feature selection*, PloS one, vol. 19, no. 7, e0307288 (2024), DOI: 10.1371/journal.pone.0307288.

[37] Aman M.M., Jasmon G.B., Bakar A.H.A., Mokhlis H., *A new approach for optimum simultaneous multi-DG distributed generation Units placement and sizing based on maximization of system loadability using HPSO (hybrid particle swarm optimization) algorithm*, Energy, vol. 66, pp. 202–215 (2014), DOI: 10.1016/j.energy.2013.12.037.